Remote Sensing Image Restoration: An Adaptive Reciprocal Cell Recovery Technique

Remote Sensing Image Restoration: An Adaptive Reciprocal Cell Recovery Technique

Chang Shu, Lihui Sun, Juanhua Li, Mengmeng Gou

Chinese Research Academy of Environmental Sciences,
No. 8, Dayangfang Beiyuan Road, Chaoyang District, Beijing, 100012, China

Corresponding author: shuchang_raes@sohu.com

Improving the quality of remote sensing images is of great value for subsequent applications. In order to reduce the noise and blur of remote sensing images, the deblurring restoration technology is studied in this paper. Firstly, the acquisition of remote sensing image and the causes of image degradation are briefly analyzed. It was found that noise, blur and aliasing had great influence on image quality. Then, based on adaptive reciprocal cell, a method of titling mode restoration is proposed, which was achieved by generating adaptive reciprocal cell, extracting effective spectrum and deblurring. In order to verify the validity of the method, TV model, ARCTV model and ARCNLM model were used to restore a synthetic image and two scene images. The results showed that the Signal Noise Ratio (SNR) of the ARCNLM model was higher than that of other models, and its mean square error (MSE) was lower than that of other models. Moreover, ARCNLM model had better deblurring effect than other models, and it could not only effectively remove aliasing, but also could maintain the texture and details of the image. The experimental results suggested the effectiveness of ARCNLM model in image restoration and provided some basis for its practical application in image restoration.

KEYWORDS: remote sensing image, image restoration, adaptive reciprocal cell.

1. Introduction

Remote sensing is a technology which is developed to detect objects in a long distance or without contact. It integrates multiple disciplines including physics, mathematics and geology [2]. In recent years, remote sensing technology has been widely applied and provided excellent methods for human observation, description and analysis of the earth, through which various important data have been obtained. The technology has been applied in many fields such as urban planning, seismic surveys, resource surveys and

missile guidance, but it has the defect of low image quality due to the limitation of imaging mechanism or atmospheric oscillation and system noise in the transmission and conversion process of image [16], which has been studied by many scientists. Papa et al. proposed a hybrid particle swarm optimization image restoration algorithm for remote sensing image restoration [10]. Yang and Ren proposed to remove the band noise in images using frequency domain notch filter, estimated the point spread function with the edge method and performed Wiener filter PSF recovery on the image [15]. Liu et al. applied the full variational method to remote sensing image restoration [5]. Marcin Gabryel et al. [7] proposed an improved Bag-of-Words algorithm. Firstly, different kinds of color histograms were obtained using Speeded-Up Robust Features (SURF) algorithm; the image classification results were significantly improved after the application of Bag-of-Words algorithm. Damasevicius et al. [4] proposed a random projection based method which identified abnormal values in 2D projection of image point features as significant image points using random projection and kernel density estimation. Compared with other methods, the method had better application value. The adaptive reciprocal cell plays a good role in image restoration. In the reciprocal cell region, the image spectrum is seldom affected by noise and aliasing; hence the image quality can be improved. Based on the adaptive reciprocal cell, the titling mode restoration method was proposed, and the effects of different models on image restoration were analyzed.

2. Remote Sensing Image Acquisition System and Degradation Reasons

Remote sensing image acquisition

The sampling system of the ground scene discretizes the reflected light after the imaging system, and then quantifies it into a digital image. Under normal circumstances, the digital image acquisition formula is:

$$I_0 = \Delta \Gamma \cdot h(f) + n. \tag{1}$$

In this equation, I_0 refers to the digital image degenerated by the imaging system, f refers to the initial image, n refers to additive noise, h refers to point spread function, showing the impact of the imaging system on the image, and Γ refers to sampling grid.

For systems with unchanged linear space, equation (1) can be written as:

$$I_0 = \Delta \Gamma \cdot (h * f) + n, \tag{2}$$

where $*$ refers to convolution calculation on the image. According to equations (1) and (2), the factors leading to the degeneration of remote sensing image can be obtained.

Noises. Noises can be found within the sensor, on the photosensitive device particles and during the quantizing process.

Blurring. Blurring is caused by the degeneration due to the spread function of point h, which is correlated with relative movement and the performance of the optical system.

Aliasing. Aliasing is induced by the inadequate spectrum expression caused by the low density of the sampling grid. In a display sampling, aliasing is inevitable.

Degradation analysis of remote sensing image acquisition system

Remote sensing image noise analysis

During imaging, various noises can appear, covering shot noise in photoelectric conversion and noise in image quantization. In this study, we assume that the image noise is Gaussian white noise [5], variance is denoted by $\acute{o}^2$, which represents the size of noises, following Gaussian distribution $\varsigma \sim (0, \acute{o}^2)$. In the whole imaging process, noises can exert great impact on image quality and disturbance on image restoration.

In equation (2), the linear expression of remote sensing image acquisition is shown, where h refers to the blurring kernel, called point spread function, which transfers to optical transfer function through Fourier transform. The model of optical transfer function is called MTF (Modulation Transfer Function) [13]. MTF characterizes the conduction properties of the optical system to the darkness of the ground scene. The MTF model curve is shown in Figure 1. Generally, $MTF \in [0,1]$, and it decreases with the increase of spatial frequency.

Figure 1
MTF curve
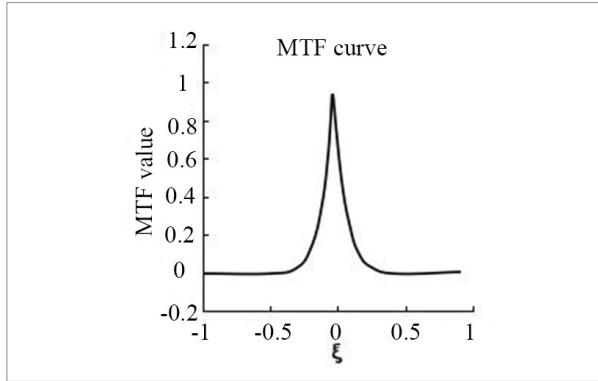
Generally, the MTF model is:

$$MTF_{sys} = MTF_{sen}MTF_{mov}MTF_{opt}, \qquad (3)$$

where MTF_{sen} refers to the detection element modulation transfer function, MTF_{mov} refers to motion blur, MTF_{opt} refers to the modulation transfer function of the optical system.

Remote sensing image aliasing analysis

The aliasing in the remote sensing image [3] has a certain connection with the sampling system, and the remote sensing image sampling uses the sampling grid. The sampling grid model is:

$$\Gamma = \{n_1 e_1 + n_2 e_2 : n_1, n_2 \in Z\} = Ze_1 + Ze_2, \qquad (4)$$

where Z refers to a set of integers; when $e_1 = (1,0)^T$ and $e_2 = (0,1)^T$, the sampling grid is a square, denoted by Γ_4 (Figure 2); when $e_1 = (1,0)^T$ and $e_2 = (1/2, \sqrt{3}/2)^T$, the sampling grid is a hexagon, denoted by Γ_6 (Figure 3).

Figure 2
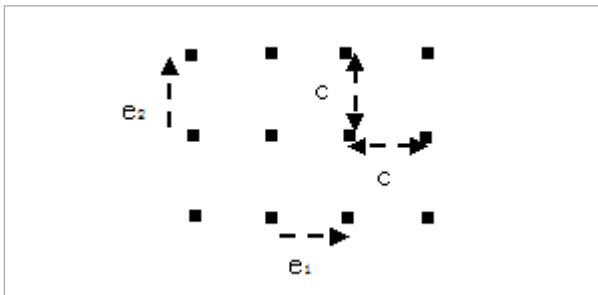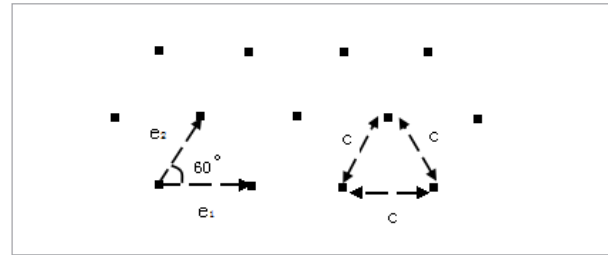Square sampling network

Figure 3
Hexagonal sampling network

Since the dual space of the real space is the Fourier space, the base vector of the real space is defined as e_1 and e_2, and the real space is divided into sampling grids. The base vector of Fourier space e_1 and e_2 is used to divide the Fourier space and form dual grids, denoted by Γ. Dual grids are generally referred to as reciprocating cells, denoted by $D^*(n)$, n refers to the specific location of each cell.

3. Adaptive Reciprocal Cell

Nominal resolution and effective resolution

The nominal resolution [11] R_{nom} refers to the length between the neighbouring sampling points. As introduced before, various aliasing and noises exist in different areas of the dual grid. However, the nominal resolution is not aware of the change on the results caused by image degradation. Therefore, the nominal resolution is changed to effective resolution [6]. When calculating with the effective resolution, weight functions need to be taken into account. The real sampling density r_{eff} and the effective resolution can be calculated with the following formulas:

$$r_{eff}(\Gamma, D^*, MTF, n, f) = \int_{D^*} z(G, G_{alias}, \hat{n})dX \qquad (5)$$

$$R_{eff}(\Gamma, D^*, MTF, n, f) = \frac{1}{\sqrt{r_{eff}(\Gamma, D^*MTF, n, f)}}. \qquad (6)$$

The expression of $z\left(G, G_{alias}, \hat{n}\right)$ is as follows:

$$z\left(G, G_{alias}, \hat{n}\right) = z\left(1, \frac{G_{alias}}{G}, \frac{\hat{n}}{G}\right) = z\left(\frac{G_{alias}}{G}, \frac{\hat{n}}{G}\right)z(a,b), \qquad (7)$$

where $a = \dfrac{G_{alias}}{\hat{G}}$ refers to the relative aliasing coefficient, $b = \dfrac{n}{G}$ refers to the relative noise coefficient. The specific weight formula is:

$$z(a,b) = \left(1 - \frac{a}{\vartheta_{alias}}\right)^{+} \left(1 - \frac{b}{\vartheta_{alias}}\right)^{+}, \qquad (8)$$

where $(s)^{+} = \max(0,s)$ refers to that the value of the equation is greater than 0, ϑ_{alias} and ϑ_{noise} are threshold values. When $a \geq \vartheta_{alias}$ or $b \geq \vartheta_{noise}$, the weight coefficient $z(a,b) = 0$. The calculation equation of relative coefficient is:

$$a^{2}\left(\tilde{X}\right) = \frac{\left|H\tilde{f}\right|_{alias}^{2}\left(\tilde{X}\right)}{\left|H\tilde{f}\right|^{2}\left(\tilde{X}\right)}, \qquad (9)$$

$$b^{2}\left(\tilde{X}\right) = \frac{|N|^{2}\left(\tilde{X}\right)}{\left|H\tilde{f}\right|^{2}\left(\tilde{X}\right)} = \frac{\sigma^{2}}{|Hf|^{2}\left(\tilde{X}\right)}, \qquad (10)$$

where σ^{2} refers to the noise level.

Adaptive reciprocal cell

In the frequency domain, the cells which restrict the shape of the reciprocal grid and tile the grid onto a plane to form a plurality of units with cell-like shapes are called reciprocal cells. In actual situation, as the aliasing of different reciprocal cells is inevitable, we introduced adaptive reciprocal cells. After the calculation of effective resolution, it can be determined that there is an area where the coefficient of aliasing and noise is smaller than the threshold value, which is called the adaptive reciprocal cell area [8]. The equation is as follows:

$$D_{adp}^{*} := \left\{\tilde{X} : a\left(\tilde{X}\right) < \vartheta_{alias} \ \ and \ \ b\left(\tilde{X}\right) < \vartheta_{noise}\right\}, \qquad (11)$$

where $\tilde{X}$ refers to frequency, $a\tilde{X}$ refers to relative aliasing, $b\tilde{X}$ refers to relative noise, ϑ_{alias} and ϑ_{noise} refer to threshold values.

4. Titling Mode Remote Sensing Image Restoration

Titling mode sampling mode and system transfer

With the successful case of the SPOT-5 satellite to obtain high-resolution images by changing sampling methods, more and more sampling methods appear. By defining c as the size of the probe element and p as the sampling pitch, the following sampling modes shown in Table 2 can be obtained.

Table 1
Sampling methods

Sampling method	Implication
The traditional sampling	$p = c$, the size of the probe element is the only condition that determines the nominal resolution.
High mode sampling mode	$p = \dfrac{c}{2}$, nominal resolution is twice that of conventional sampling.
Titling mode sampling	The angle between the detection linear array and the satellite flight direction is θ, $p = c\sin(\theta)$, i.e., nominal resolution is $\dfrac{1}{\sin(\theta)}$ times that of conventional sampling.
Hexagonal sampling	$p = c\sqrt{\dfrac{4}{3}}\sin(\theta)$, i.e., nominal resolution is $\dfrac{1}{\sqrt{\dfrac{4}{3}}\sin(\theta)}$ times that of conventional sampling.

As high modulus sampling requires two detection linear arrays with complex hardware and hexagonal sampling method has some difficult technical problems, we adopted titling sampling mode, which uses square sampling grid to obtain titling remote sensing images. Although the titling can be corrected by the interpolation method, this can cause unnecessary energy loss of the remote sensing image. The imaging system MTF model in this mode is:

$$\left(MTF_{sys}\right)_{\theta,n} = 4p^{2}e^{-p\sqrt{a_{1}\xi^{2}+a_{2}\eta^{2}}}\,e^{-p\beta\left|\zeta\cos\theta - \eta\sin\theta\right|} \qquad (12)$$

where $p = c\sin(\theta)$ and β refers to the conductivity parameter, a_1 and a_2 refer to optical system performance coefficients.

Steps of the titling method

Aiming at the characteristics of adaptive reciprocal cells, we choose the titling mode remote sensing image restoration method. The working framework of titling mode restoration is shown in Figure 4.

Figure 4

The working framework of titling mode restoration
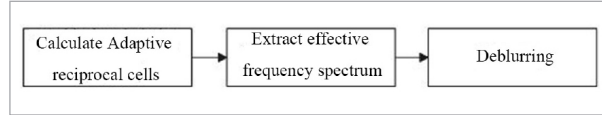
1 Calculate the adaptive reciprocal cells of the imaging system

2 Extract the effective frequency. Extend the spectrum of the image in the frequency domain and find the information contained in the active spectrum in the coverage area by the adaptive reciprocal cell.

3 Deblurring.

Deblurring method

Image restoration is an inverse problem that can be solved by regularization techniques [12]. Usually the equation of regularization method is:

$$\hat{f} = \arg\min_I \left\{ \Re(I) + \frac{\beta}{2}\cdot\|I_0 - h(I)\|^2 \right\}. \tag{13}$$

In the equation, the first term is a regular term; the second is a data fidelity item; β is a regularization parameter; $\Re(I)$ can be taken as a low pass filter to make the image smooth and play a filtering role.

Non-local regularization method

Non-local average filtering method is adopted to transfer the regularization method from local one to non-local one [14]. In the actual operation, the simplified form can be used as follows:

$$I^{n+1} = I^n + dt\left(\frac{\int z(X,Y)I(Y)dY}{\int z(X,Y)dY} + \beta F^-\left(W^*\left(\hat{I}_0 - W\hat{I}\right)\right)\right). \tag{14}$$

The specific steps are as follows.

1 Before iteration, the previous two steps were performed on the image to obtain image I_0 as the initial value. According to $r(n) = Mean\left(\left|I^n - I^{n-1}\right|\right)$, time step size and iterative convergence conditions were calculated.

2 The image I_0 after n times of iteration was transferred to Fourier domain. Then, $W^*\left(\hat{I}_0 - W\hat{I}\right)^n$ was calculated and transferred to airspace through inverse Fourier transform.

3 Calculate the nth non-local mean filter value.

4 Based on Euler-Lagrange equation, the image I^n was updated to I^{n+1}.

5 Judge whether the iteration met the conditions, if yes, end; if no, repeat steps (2) to (4) until the conditions were met.

TV regularization method

Usually, the TV regularization model is as follows.

$$\tilde{I} = \arg\ \min_I \left\{ \|\nabla I\| + \frac{\beta}{2}\cdot\|h(I) - I_0\|^2 \right\}, \tag{15}$$

where I_0 refers to the degeneration image to be restored, I refers to the restored image, β refers to the fidelity coefficient. To achieve better restoration effect, we changed the fidelity term to the Fourier domain and obtained the following equation.

$$\tilde{I} = \arg\min_I \left\{ \|\nabla I\| + \frac{\beta}{2}\cdot\int_\Omega \left[\tilde{H}\tilde{I} - I_0\right]^2 d\tilde{X} \right\}, \tag{16}$$

where $\hat{\Omega} = \left[-0.5, 0.5\right]^2$ refers to Fourier spectrum support rate, $\hat{I}$ and $\hat{I}_0$ refer to the Fourier spectrum of I and I_0, $\tilde{X} = (\xi, \eta)$ refers to Fourier coordinates, $\hat{H}$ refers to the system MTF. In calculation, $\hat{\Omega}$ refers to the reciprocal cell D^*. In addition, D^*_{adp} can be taken as a projection factor, then the following equation can be obtained:

$$\tilde{I} = \arg\min_U \left\{ \|\nabla I\| + \frac{\beta}{2}\cdot\left\|P\hat{H}\hat{I} - \hat{I}_0\right\|^2 \right\}, \tag{17}$$

where $P = \chi_{D\ adp}$, χ is a membership function. Then, the corresponding Euler-Lagrange equation is

$$-div\left(\frac{\nabla I}{\|\nabla I\|}\right)+\beta \hat{H}^* P^*\left(P\hat{H}\hat{I}-\hat{I_0}\right)=0, \qquad (18)$$

where $*$ refers to complex conjugate [1], $W^*=\hat{H}^* P^*$, $W=\hat{H}P$. Then, the above equation can be simplified as:

$$-div\left(\frac{\nabla I}{\|\nabla I\|}\right)+\beta W^*\left(W\hat{I}-\hat{I_0}\right)=0. \qquad (19)$$

By using the gradient descent method, the corresponding partial differential equation is obtained:

$$\begin{cases} \dfrac{\partial I}{\partial t}=div\left(\dfrac{\nabla I}{\|\nabla I\|}\right)+\beta F^-\left(W^*\left(\hat{I_0}-W\hat{I}\right)\right) \\[2mm] \qquad \dfrac{\partial I}{\partial r}=0, on \quad \partial\Omega \\[2mm] \qquad I(X,Y,0)=I_0 \end{cases}, \qquad (20)$$

where $F^-(.)$ refers to inverse Fourier transform, $\partial\Omega$ refers to image boundary, r refers to the normal vector of $\partial\Omega$, $\frac{\partial I}{\partial n}=0$ refers to that the spread meets the Neumann boundary condition, and I_0 refers to the initial value.

The specific steps are as follows:

1 Perform the previous 2 steps on the image and obtain the convergence condition of the iteration as follows:

$$r(n)=Mean\left(\left\|I^n-I^{n-1}\right\|\right). \qquad (21)$$

The equation represents the average value of the gray scale change absolute values of the nth iteration and the previous result.

2 Transfer the image I^n after n times of iteration to Fourier domain and calculate $W*\left(\hat{I_0}-W\hat{I}^n\right)$ and transfer it to the airspace.

3 Calculate the nth total variation flow.

4 Update the image I^n to I^{n+1}.

5 Judge whether the iteration met the conditions, if yes, end; if not, repeat steps ② to ④ until the conditions were met.

Experiment and analysis

Experimental purpose

In this paper, experiments were carried out on a composite graph and two scene graphs to compare the deblurring effect of the three models. The SNR and the mean square error MSE are used to quantify the denoising effect.

Experimental parameters

The experimental results run on Windows XP operating system and Matlab8.0 software. Two sets of images of the same size are selected for testing. Firstly, MTF is used to perform deblurring on the images. In the process of algorithm implementation, the test images are divided into overlapping images (9×9). In an iteration, the initial value of β is set to 4 and the end value of iteration is set to 2; the value of λ is $0.05/\max\left(\sigma^2,10^{12}\right)$, the value of α should be smaller than λ, then, $\alpha=0.9\lambda$.

Experimental procedures

1 Perform titling simulation on the image, added with various degeneration factors.

2 Perform primary elimination of aliasing on the image based on titling mode restoration framework.

3 Restore the image with the ARCTV model and record data.

4 Restore the image with the ARCNLM model and record data.

Experimental results

The results of the three methods are shown in Figures 4 and 5.

Figure 5 is the restoration result of the synthesized image. Figure 5a is the original image and Figure 5b is the titling mode simulation image with degeneration factor. It could be seen that the image quality was seriously degraded. After deblurred by TV model (Figure 5c), aliasing still existed in the picture, but after deblurring by ARCTV model (Figure 5d), aliasing was obviously removed. After deblurred by ARCNLM model (Figure 5e), aliasing phenomenon was removed, and moreover image edge and diagonal line became clearer. It indicated that the model could not only remove the aliasing phenomenon, but also maintained the texture and details of the image, which made the image clearer.

Figure 5

A comparison of composite image recovery results (a) initial image, (b) simulated degraded image, (c) deblurring result of TV model, (d) deblurring result of ARCTV model, (e) deblurring result of ARCNLM model

a

b

c

d

e
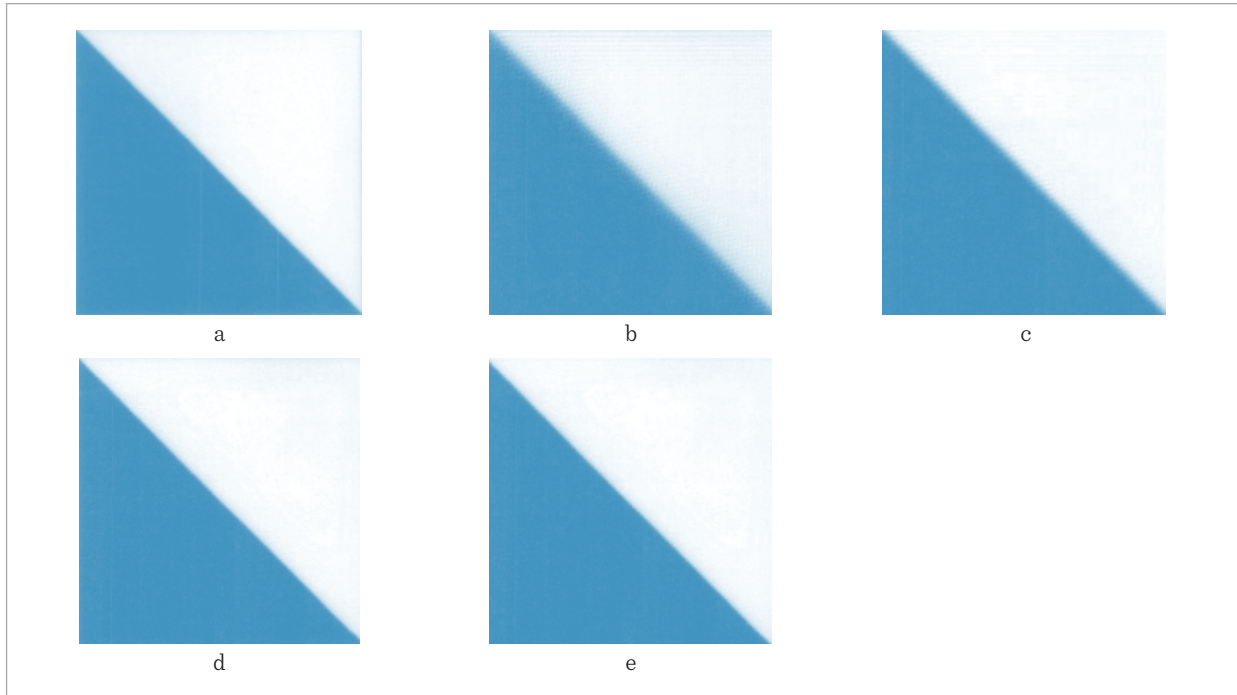
Figure 6

A comparison of the restoration results of the first scene image initial stage, (b) simulated degraded image, (c) deblurring result of TV model, (d) deblurring result of ARCTV model, (e) deblurring result of ARCNLM model
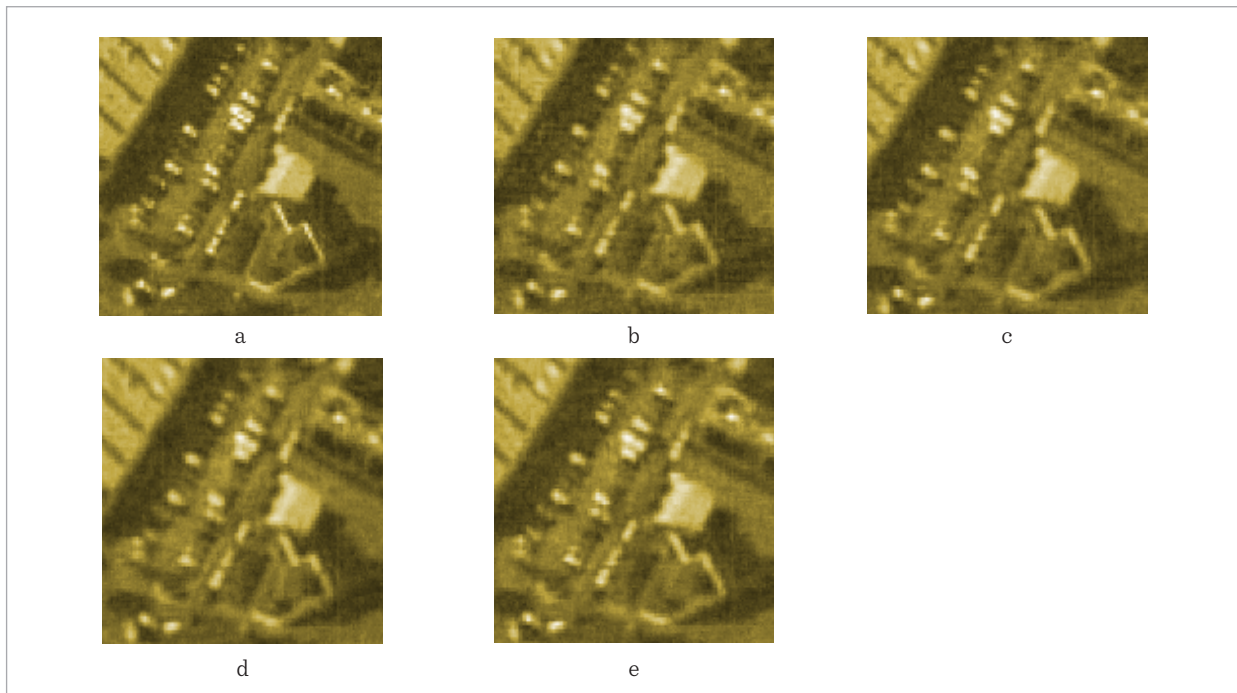

a

b

c

d

e

Figure 6 is the restoration result of the scene image. Figure 6a is the original image. After adding degradation factors, the image quality becomes worse obviously (Figure 6b). After deblurred by TV model, the aliasing phenomenon was not removed (Figure 6c). After deblurred by ARCTV and ARCNLM models, the aliasing and noise were removed, and the restoration result was good (Figures 6d and 6e). After deblurred by the ARCNLM model, the edge and texture of the image were maintained, and the deblurring effect was clear and natural (Figure 6e).

The measured data of the three methods are shown in Tables 2 and 3.

Table 2
SNR comparison of the three methods

	TV	ARCTV	ARCNLM
Figure 4	25.5	34.2	43.5
Figure 5	19.8	24.6	29.4

Table 3
MSE comparison of the three methods

|	TV	ARCTV	ARCNLM
Figure 4	67.7	15.4	2.5
Figure 5	65.4	22.3	15.1

It was found that the SNR of the ARCNLM model was higher than that of the TC and ARCTV model, and its MSE value was much less than that of the other two models, indicating the effectiveness of ARCNLM in restoring images.

To further verify the restoration effect of ARCNLM model, an image with large texture density and multiple local details was taken for restoration. The results are shown in Figure 7.

Figure 7 shows the restoration of the second scene image. Figure 7I is the original image. Figure 7II is the image after degradation factor was added; it was found that the details of the image had great loss. The comparison of Figures 7III and 7IV suggested that the details of the image restored well and the texture was complete when ARCNLM model was used, indicating ARCNLM model was better than ARCTV model in restoring images.

Figure 7

Comparison of restoration results of the second scene image original image; II. simulated degraded image; III. denoising result of ARCTV model; IV. denoising result of ARCNLM model

I

II

III

IV
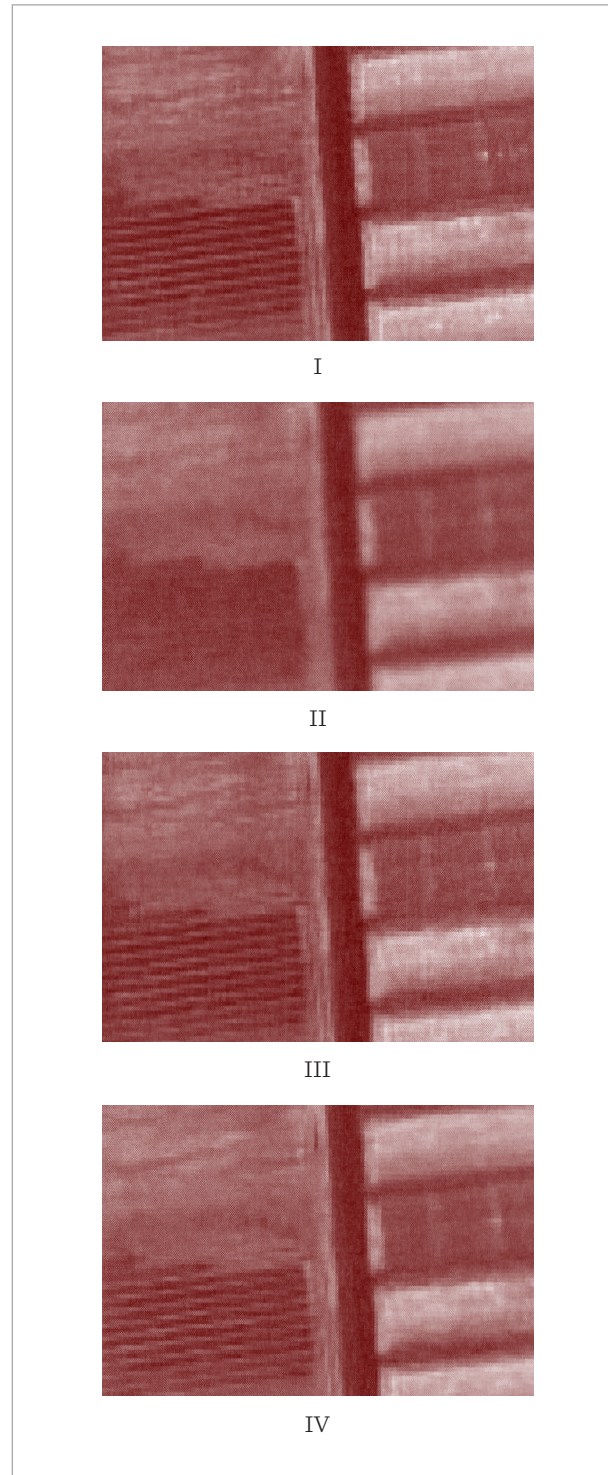
5. Discussion

Degradation factors of remote sensing image mainly include noise, blur and aliasing, which have a great impact on image quality. The adaptive reciprocal cell is seldom affected by noise and aliasing and has a better performance in image restoration. Based on the analysis of adaptive reciprocal cell, a titling mode based image restoration method which included procedures of calculation of adaptive reciprocal cell, extraction of effective spectrum and deblurring is proposed.

On the basis of the titling mode based adaptive reciprocal cell, a TV regularization model was proposed firstly. Then, in order to further improve the image restoration ability, ARCTV model and ARCNLM model were also proposed. In order to compare the restoration effect of the three models, a synthesized image and a scene image were restored using the three models in the environment of Windows XP operation system and Matlab8.0 software.

It could be found from Figures 5 and 6 that the resolution of the image was greatly reduced and the image quality is greatly affected by the degradation factors. After deblurring using the TV model, the aliasing phenomenon still existed in the image and had not been effectively eliminated. Compared with the TV regularization model, non-local regularization model can not only effectively remove noise, but also preserve the texture and edge details of the image. The deblurring result of the synthetic image clearly suggested that the ARCNLM model made the edges and diagonal lines clearer, indicating that the model had better deblurring effect. It could be seen from the data measurement results that the ARCNLM model had higher SNR value and smaller MSE value, indicating the good image restoration ability of the model.

6. Conclusion

Adaptive reciprocal cell is effective in restoring images. Based on it, this study put forward titling mode restoration method and compared the restoration effects of TV model, ARCTV model and ARCNLM model. The results showed that the ARCNLM model could effectively remove noise and aliasing, while maintaining the texture and edge details of the image. Compared with the other models, the ARCNLM model had higher SNR value and smaller MSE, which indicated that the ARCNLM model had better image restoration ability and had strong practicability and feasibility in restoration of remote sensing images, but there are many problems in the restoration of the actual remote sensing image which need to be solved. Further research is needed to make this method serve image restoration better.

References

1. Blaga Adara, M., Crasmareanu, M. The geometry of complex conjugate connections. Hacettepe University Bulletin of Natural Sciences & Engineering, 2012, 41(1), 119-126. https://doi.org/10.5644/SJM.10.2.09

2. Blaschke, T. Object based image analysis for remote sensing. ISPRS Journal of Photogrammetry & Remote Sensing, 2010, 65(1), 2-16. https://doi.org/10.1016/j.isprsjprs.2009.06.004

3. Chabert, M., Lacaze, B. Non uniform sampling for remote sensing images. 2012 IEEE International Geoscience and Remote Sensing Symposium, Munich, Germany, July 22-27, 2012, 88(8), 4718-4721. https://doi.org/10.1109/IGARSS.2012.6352339

4. Damasevicius, R., Maskeliunas, R., Wozniak, M., Polap, D., Sidekerskiene, T., Gabryel, M. Detection of Saliency Map as Image Feature Outliers Using Random Projections Based Method. 13th International Computer Engineering Conference, 2017, 85-90. https://doi.org/10.1109/ICENCO.2017.8289768

5. Daqaq, M. F. Transduction of a Bistable Inductive Generator Driven by White and Exponentially Correlated Gaussian Noise. Journal of Sound & Vibration, 2011, 330(11), 2554-2564. https://doi.org/10.1016/j.jsv.2010.12.005

6. Frehlich, R., Sharman, R. The Use of Structure Functions and Spectra from Numerical Model Output to Determine Effective Model Resolution. Monthly Weather Review, 2011, 136(136), 1537. https://doi.org/10.1175/2007MWR2250.1

7. Gabryel M., Damaševičius R. The Image Classification with Different Types of Image Features. In: Rutkowski L., Korytkowski M., Scherer R., Tadeusiewicz

R., Zadeh L., Zurada J. (Eds.) Artificial Intelligence and Soft Computing. ICAISC 2017, Lecture Notes in Computer Science, 2017, 10245, 497-506. https://doi.org/10.1007/978-3-319-59063-9_44

8. He, Y., Zhang, J., Wang, S., Zheng, Y. H., Wang, H., Chen, Y. J. Sparse Representation Based Satellite Image Restoration Using Adaptive Reciprocal Cell. International Journal of Multimedia & Ubiquitous Engineering, 2014, 9(10), 341-348. https://doi.org/10.14257/ijmue.2014.9.10.33

9. Liu, P., Zhang, Y. W., Lu, C. Selection of Regularization Parameter Based on Generalized Cross-Validation in Total Variation Remote Sensing Image Restoration. Proceedings of SPIE – The International Society for Optical Engineering, 2010, 7830(24), 78301P-78301P-7. https://doi.org/10.1117/12.868615

10. Papa, J. P., Fonseca, L. M. G., de Carvalho, L. A. S. Projections Onto Convex Sets Through Particle Swarm Optimization and Its Application for Remote Sensing Image Restoration. Pattern Recognition Letters, 2010, 31(13), 1876-1886. https://doi.org/10.1016/j.patrec.2010.02.012

11. Wang, C, Hitzler, P. A Resolution Procedure for Description Logics with Nominal Schemas. Semantic Technol-ogy. Springer Berlin Heidelberg, 2013, 1-16. https://doi.org/10.1007/978-3-642-37996-3_1

12. Wang, Y., Qiao, X., Li, X., Meng, L. Regularization Method of Inverse Problems in Image Information Processing. Journal of Convergence Information Technology, 2013, 8(7), 966-974. https://doi.org/10.4156/jcit.vol8.issue7.119

13. Wang, Z. L., Li, B., Zhang, Y., Xiao, H. S., Zhou, C. H. Satellite Vibration on Image Quality Degradation of Remote Sensing Camera. Research on Precision Instrument & Machinery, 2012, 1(1), 6-10.

14. Werlberger, M., Pock, T., Bischof, H. Motion Estimation with Non-Local Total Variation Regularization. Computer Vision and Pattern Recognition, San Francisco, CA, USA, June 2010, 2464-2471.

15. Yang, L., Ren, J. Remote Sensing Image Restoration Using Estimated Point Spread Function. International Conference on Information NETWORKING and Automation, Kunming, China, Oct. 2010, V1-48 - V1-52.

16. Zhang, F.Y. No-Reference Remote Sensing Image Quality Assessment Based on Natural Scene Statistical in Wavelet Domain. Journal of Electronics & Information Technology, 2011, 33(11), 2742-2747. https://doi.org/10.3724/SP.J.1146.2011.00491